Bistability and self-pulsation phenomena in silicon microring resonators based on nonlinear optical effects

Shaowu Chen,* Libin Zhang, Yonghao Fei, and Tongtong Cao

State Key Laboratory on Integrated Optoelectronics, Institute of Semiconductors, Chinese Academy of Sciences, Beijing 100083, China

swchen@semi.ac.cn

Abstract: Bistability (BS) and self-pulsation (SP) phenomena in silicon microring resonators (MRR) with intense CW light injection are studied. Several nonlinear optical effects including Kerr effect, two-photon absorption, free carrier absorption and free carrier dispersion are taken into account. The threshold optical intensity of BS and SP is derived from the coupled mode theory and a linear stability analysis method. The influences of MRR's parameters (carrier lifetime, linear loss and radius) and light injection conditions (input power, wavelength detuning) on the characteristics of SP (modulation depth and oscillating frequency) are analyzed and discussed. It is shown that, SP occurs only if the carrier lifetime ranges from several ps to several-hundred ps and the input light intensity is higher than 10^6W/cm^2. The modulation depth of SP can be as large as 8dB and the associated oscillating frequency is in the range from several GHz to beyond 10 GHz.

OCIS codes: (190.1450) Bistability; (190.3100) Instability and chaos; (190.4390) Nonlinear optics, integrated optics; (190.5940) Self-action effects; (230.1150) All-optical devices; (230.4555) Coupled resonators.

References and links

1. R. G. Harrison and D. J. Biswas, "Chaos in light," Nature **321**(6068), 394–401 (1986).
2. V. Grigoriev and F. Biancalana, "Bistability, multistability and non-reciprocal light propagation in Thue–Morse multilayered structures," New J. Phys. **12**(5), 053041 (2010).
3. A. Parini, G. Bellanca, S. Trillo, M. Conforti, A. Locatelli, and C. D. Angelis, "Self-pulsing and bistability in nonlinear Bragg gratings," J. Opt. Soc. Am. B **24**(9), 2229–2237 (2007).
4. V. Grigoriev and F. Biancalana, "Resonant self-pulsations in coupled nonlinear microcavities," Phys. Rev. A **83**(4), 043816 (2011).
5. B. Maes, M. Fiers, and P. Bienstman, "Self-pulsing and chaos in short chains of coupled nonlinear microcavities," Phys. Rev. A **80**(3), 033805 (2009).
6. A. Sterkhova, J. Luksch, and J. Petracek, "Simulation of self-pulsing and chaos in coupled microring resonators," in *Proceedings of 12th International Conference on Transparent Optical Networks (ICTON),* (Munich, Germany, 2010), paper Mo.P.19. *http://ieeexplore.ieee.org/xpls/abs_all.jsp?arnumber=5549300*
7. G. Priem, P. Dumon, W. Bogaerts, D. V. Thourhout, G. Morthier, and R. Baets, "Nonlinear effects in ultrasmall Silicon-on-Insulator ring resonators," Proc. SPIE **6183**, 61831A, 61831A-8 (2006).
8. G. Priem, P. Dumon, W. Bogaerts, D. Van Thourhout, G. Morthier, and R. Baets, "Optical bistability and pulsating behaviour in Silicon-On-Insulator ring resonator structures," Opt. Express **13**(23), 9623–9628 (2005).
9. Q. Xu and M. Lipson, "Carrier-induced optical bistability in silicon ring resonators," Opt. Lett. **31**(3), 341–343 (2006).
10. K. Ikeda, "Multiple-valued stationary state and its instability of the transmitted light by a ring cavity system," Opt. Commun. **30**(2), 257–261 (1979).
11. K. Ikeda, H. Daido, and O. Akimoto, "Optical turbulence: chaotic behavior of transmitted light from a ring cavity," Phys. Rev. Lett. **45**(9), 709–712 (1980).
12. K. Ikeda and O. Akimoto, "Instability leading to periodic and chaotic self-pulsations in a bistable optical cavity," Phys. Rev. Lett. **48**(9), 617–620 (1982).

#160644 - $15.00 USD Received 3 Jan 2012; revised 16 Feb 2012; accepted 14 Mar 2012; published 19 Mar 2012

13. H. M. Gibbs, F. A. Hopf, D. L. Kaplan, and R. L. Shoemaker, "Observation of chaos in optical bistability," Phys. Rev. Lett. **46**(7), 474–477 (1981).
14. F. Morichetti, A. Melloni, J. Čáp, J. Petráćek, P. Bienstman, G. Priem, B. Maes, M. Lauritano, and G. Bellanca, "Self-phase modulation in slow-wave structures: A comparative numerical analysis," Opt. Quantum Electron. **38**(9-11), 761–780 (2007).
15. J. Petráček, A. Sterkhova, and J. Luksch, "Numerical scheme for simulation of self-pulsing and chaos in coupled microring resonators," Microw. Opt. Technol. Lett. **53**(10), 2238–2242 (2011).
16. S. Malaguti, G. Bellanca, A. de Rossi, S. Combrié, and S. Trillo, "Self-pulsing driven by two-photon absorption in semiconductor nanocavities," Phys. Rev. A **83**(5), 051802 (2011).
17. M. Tabor, *Chaos and integrability in nonlinear dynamics: an introduction* (Wiley, New York, 1989).
18. P. Chamorro-Posada, P. Martin-Ramos, J. Sánchez-Curto, J. C. García-Escartín, J. A. Calzada, C. Palencia, and A. Durán, "Nonlinear Bloch modes, optical switching and Bragg solitons in tightly coupled micro-ring resonator chains," J. Opt. **14**(1), 015205 (2012).
19. R. Dekker, N. Usechak, M. Först, and A. Driessen, "Ultrafast nonlinear all-optical processes in silicon-on-insulator waveguides," J. Phys. D Appl. Phys. **40**(14), R249–R271 (2007).
20. J. Leuthold, C. Koos, and W. Freude, "Nonlinear silicon photonics," Nat. Photonics **4**(8), 535–544 (2010).
21. H. A. Haus, M. A. Popovic, M. R. Watts, C. Manolatou, B. E. Little, and S. T. Chu, "Optical resonators and filters," in *Optical Microcavities*, Kerry Vahala, ed. (World Scientific, Singapore, 2004).
22. A. D. Rossi, M. Lauritano, S. Combrié, Q. V. Tran, and C. Husko, "Interplay of plasma-induced and fast thermal nonlinearities in a GaAs-based photonic crystal nanocavity," Phys. Rev. A **79**(4), 043818 (2009).
23. V. Van, T. A. Ibrahim, P. P. Absil, F. G. Johnson, R. Grover, and P. T. Ho, "Optical signal processing using nonlinear semiconductor microring resonators," IEEE J. Sel. Top. Quantum Electron. **8**(3), 705–713 (2002).
24. B. E. Little, S. T. Chu, H. A. Haus, J. Foresi, and J.-P. Laine, "Microring resonator channel dropping filters," J. Lightwave Technol. **15**(6), 998–1005 (1997).
25. R. A. Soref and B. R. Bennett, "Electrooptical effects in silicon," IEEE J. Quantum Electron. **23**(1), 123–129 (1987).
26. P. Rabier and W. H. Steier, "Polymer microring resonators," in *Optical Microcavities*, Kerry Vahala, ed. (World Scientific, Singapore, 2004).
27. Q. Lin, O. J. Painter, and G. P. Agrawal, "Nonlinear optical phenomena in silicon waveguides: Modeling and applications," Opt. Express **15**(25), 16604–16644 (2007).
28. H. K. Tsang and Y. Liu, "Nonlinear optical properties of silicon waveguides," Semicond. Sci. Technol. **23**(6), 064007 (2008).
29. A. C. Turner-Foster, M. A. Foster, J. S. Levy, C. B. Poitras, R. Salem, A. L. Gaeta, and M. Lipson, "Ultrashort free-carrier lifetime in low-loss silicon nanowaveguides," Opt. Express **18**(4), 3582–3591 (2010).
30. M. Först, J. Niehusmann, T. Plötzing, J. Bolten, T. Wahlbrink, C. Moormann, and H. Kurz, "High-speed all-optical switching in ion-implanted silicon-on-insulator microring resonators," Opt. Lett. **32**(14), 2046–2048 (2007).
31. M. Waldow, T. Plötzing, M. Gottheil, M. Först, J. Bolten, T. Wahlbrink, and H. Kurz, "25ps all-optical switching in oxygen implanted silicon-on-insulator microring resonator," Opt. Express **16**(11), 7693–7702 (2008).
32. B. Jalali, V. Raghunathan, R. Shori, S. Fathpour, D. Dimitropoulos, and O. Stafsudd, "Prospects for silicon mid-IR raman lasers," IEEE J. Sel. Top. Quantum Electron. **12**(6), 1618–1627 (2006).

1. Introduction

Optical bistability (BS) and self-pulsation (SP) have been demonstrated theoretically and experimentally in various photonic devices with nonlinear responses and feedbacks [1], such as Fabry-Perot resonators [2], fiber Bragg gratings [3, 4], photonic crystal micro-cavities [5] and microring resonators [6–9], etc. It has been indicated that SP results from two competing mechanisms, e.g., the relaxation time of the nonlinear medium and the transit time of the light [10–13]. K. Ikeda has shown theoretically that SP or even chaos can be observed under two opposite extreme conditions: the relaxation time of the medium is much shorter or much longer than the transit time [11, 12].

Two methods are widely used for analyzing BS and SP: Finite-Difference Time-Domain (FDTD) method [14, 15] and Coupled Mode Theory (CMT) [3–5, 16]. Though FDTD is an accurate method and is capable to handle with both linear and nonlinear features in photonic devices, it is inadequate to reveal physics insights of BS and SP phenomena. On the other hand, CMT provides an intuitive way to define the criteria for BS and SP boundaries through the linear stability analysis of differential equations or Hopf bifurcation method [17]. Current analysis of BS and SP phenomena by CMT method is mainly focused on the Kerr effect in photonic crystal cavities. Comparing with photonic crystals, silicon microring resonators (MRR) have the characteristics of smaller Kerr, smaller TPA coefficients, and a longer carrier

#160644 - $15.00 USD Received 3 Jan 2012; revised 16 Feb 2012; accepted 14 Mar 2012; published 19 Mar 2012

lifetime, which indicate that MRRs need a higher input power to excite SP. Although the TPA effect has been discussed in detail in [16], the Kerr effect which also plays a role in the threshold input power values for SP, was omitted completely. Other numerical methods such as discrete nonlinear Bloch modes can be used to analyze the nonlinear phenomena as well [18].

In this paper, we use a silicon MRR with an all-pass configuration (see Fig. 1) to obtain a better understanding of physical and mathematical pictures of BS and SP phenomena with the consideration of the Kerr effect, TPA effect, free carrier absorption (FCA) effect and free carrier dispersion (FCD) effect [19, 20].

In section 2, the nonlinear light propagation equation and the carrier density rate equation for the silicon MRR using CMT method are established. In section 3, through linear stability analysis of the established differential equations, BS and SP phenomena are analyzed. The effects of several key parameters, such as the carrier lifetime, the input light intensity, the input light wavelength detuning, and the linear loss of the MRR are investigated in detail. The dependence of modulation depth of SP as well as its oscillating frequency on the input light intensity is also discussed. Finally, we conclude our paper in section 4.

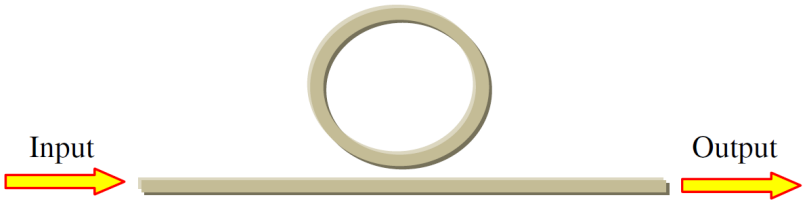

Fig. 1. Configuration of an all-pass microring resonator.

2. Numerical model

The nonlinear light propagation equation derived from a nonlinear coupled-mode theory and carrier density rate equation are used to analyze SP and BS phenomena in the all-pass MRR (Fig. 1). Under linear condition, the coupled mode theory has been demonstrated to agree very well with the FDTD method [21]. The nonlinear equations considering Kerr effect, Two Photon Absorption (TPA) effect, Free-Carrier Absorption (FCA) effect and the associated Free-Carrier Dispersion (FCD) effect are given by [21–24]:

$$\frac{\partial u}{\partial t}=\left\{i\left(\omega_0-\omega_L\right)-i\frac{\omega_0}{n_0}\left[\frac{n_{2I}c}{n_0V_{Kerr}}|u|^2-\left(\sigma_{r1}N+\sigma_{r2}N^{0.8}\right)\right]-\left(\frac{\omega_0}{2Q_L}+\frac{\beta_2c^2}{2n_0^2}\frac{|u|^2}{V_{TPA}}+\frac{\sigma_{FCA}Nc}{2n_0}\right)\right\}u+\sqrt{\Gamma_cP_{in}}, \tag{1}$$

$$\frac{\partial N}{\partial t}=\frac{\beta_2}{2\hbar\omega}I^2-\frac{N}{\tau_{car}}=\frac{c^2\beta_2}{n_0^2\,2\hbar\omega_0V_{TPA}V_{car}}|u|^4-\frac{N}{\tau_{car}}. \tag{2}$$

Here u is the complex amplitude of light propagating in the MRR, which is normalized by letting $|u|^2$ equal to the mode energy; P_{in} is the incident power in the straight silicon waveguide; ω_0 is the resonance frequency of the MRR and ω_L is the incident light frequency; $n_{2I}c|u|^2/(n_0V_{Kerr})$ is the refractive index change caused by the Kerr effect, where n_{2I} is the Kerr coefficient and V_{Kerr} the Kerr nonlinear volume; $-\left(\sigma_{r1}N+\sigma_{r2}N^{0.8}\right)$ is the refractive index change induced by FCD [25]; $\omega_0/(2Q_L)$ refers to the linear loss and Q_L is the loaded

#160644 - $15.00 USD Received 3 Jan 2012; revised 16 Feb 2012; accepted 14 Mar 2012; published 19 Mar 2012

quality factor of the MRR which is defined as $Q_L = \lambda_0 / \Delta\lambda_{3dB}$; $\beta_2 c^2 |u|^2 / (2n_0^2 V_{TPA})$ is the absorption loss caused by TPA with β_2 being the TPA coefficient; $\sigma_{FCA} Nc/(2n_0)$ is the FCA loss with σ_{FCA} being the FCA coefficient; $\sqrt{\Gamma_c P_{in}}$ is the energy coupled into the MRR where Γ_c is the coupling coefficient and is related to the external quality factor Q_e by $\Gamma_c = \omega_0 / Q_e$. In Eq. (2), the first term on the right hand is the free carrier density change induced by TPA, and the second term is the dissipation of free carrier density caused by free carrier recombination where τ_{car} is the free carrier lifetime.

Under critical coupling condition, the inner quality factor Q_0 is equal to the external quality factor Q_e, which means that the power loss in the MRR is equal to the power coupled into the ring via the coupler. Because $1/Q_L \equiv 1/Q_0 + 1/Q_e$, we get $2Q_L = Q_0$. It has been shown that Q_0 is related to the linear loss coefficient α [m^{-1}] by $Q_0 = \frac{\pi L n_0}{\lambda_0} \frac{\sqrt{a}}{1-a}$,where $a = \exp(-\alpha L/2)$. Since $\alpha L << 1$, we get $a \approx 1 - \alpha L/2$ and $Q_0 \approx \frac{2\pi n_0}{\alpha \lambda_0}$ [26].

In the output port of the MRR, light obeys the following equation [21]

$$b_{output} = \sqrt{P_{in}} - \sqrt{\Gamma_c} u, \tag{3}$$

where b_{output} is the complex amplitude of the output light which has been normalized such that $|b_{output}|^2$ is equal to the output power.

It has been proved that the stability of the differential equations Eqs. (1) and (2) can be analyzed by using Hopf bifurcation method which uses linear matrix to find the eigenvalues. The matrix can be obtained by two steps: finding the values that satisfy stable conditions $\partial u/\partial t = 0, \partial N/\partial t = 0$; adding small perturbations to these stable values and substituting the updated results into the differential equations, with omitting higher order terms and obtaining the linear matrix. It should be noted that we should normalize Eqs. (1) and (2) to make the values of parameters in the same order of magnitude as much as possible to facilitate the procedure to get the correct eigenvalues of the matrix.

The normalized dimensionless nonlinear transmission function as well as normalized dimensionless carrier density rate equation are as follows [16]:

$$\frac{\partial a}{\partial t} = \sqrt{P} + i\delta a - i n_{Kerr\_N} |a|^2 a + i(n + \sigma_{FCD} n^{0.8}) a - (1 + \gamma_{FCA} n) a - \alpha_{TPA} |a|^2 a, \tag{4}$$

$$\frac{\partial n}{\partial t} = |a|^4 - \frac{n}{\tau}. \tag{5}$$

where the normalized time t is in unit of $1/\Gamma_0$ with $\Gamma_0 = \omega_0/(2Q_L)$. $|a|^2 = |u|^2 \sqrt{\sigma\beta}$ is the normalized energy in the ring; $P = \frac{\sqrt{\sigma\beta}\Gamma_c}{\Gamma_0^2} P_{in}$ is the normalized input power; $n = \sigma N$ is the normalized carrier density; $\delta = \frac{\omega_0 - \omega_L}{\Gamma_0}$ is the normalized input light frequency detuning; $n_{Kerr\_N} = \frac{\omega_0 n_{2I} c}{\Gamma_0 n_0^2 V_{Kerr} \sqrt{\sigma\beta}}$ is the Kerr nonlinearity; $\sigma \equiv \sigma_{r1} \frac{\omega_0}{n_0 \Gamma_0}$ and $\sigma_{FCD} = \frac{\omega_0}{n_0 \Gamma_0} \frac{\sigma_{r2}}{\sigma^{0.8}}$ are

#160644 - $15.00 USD Received 3 Jan 2012; revised 16 Feb 2012; accepted 14 Mar 2012; published 19 Mar 2012

related to the FCD effect; $\alpha_{TPA} = \dfrac{\beta_2 c^2}{2n_0^2\Gamma_0 V_{TPA}\sqrt{\sigma\beta}}$ is the TPA coefficient; $\gamma_{FCA} = \dfrac{\sigma_{FCA} c}{2n_0\Gamma_0\sigma}$ is the FCA absorption coefficient; $\tau = \Gamma_0\tau_{car}$ is the carrier lifetime; and $\beta \equiv c^2\beta_2 / (\Gamma_0 2\hbar\omega_0 n_0^2 V_{TPA} V_{car})$.

The equation to describe the dimensionless normalized output light in the through port of the MRR is similar to Eq. (3). It only needs to replace the real parameters P_{in} and u in Eq. (3) with dimensionless normalized parameters P and a, respectively.

Equations (4) and (5) have steady state solutions $a(t) = A, n(t) = N_0$ by letting $\partial a / \partial t = 0$ and $\partial n / \partial t = 0$:

$$N_0 = \tau \mid A \mid^4 = \tau E^2, \tag{6}$$

$$P = E\left[\left(1 + \gamma_{FCA}\tau E^2 + \alpha_{TPA} E\right)^2 + \left(\delta - n_{Kerr\_N} E + \tau E^2 + \sigma_{FCD}\tau^{0.8} E^{1.6}\right)^2\right]. \tag{7}$$

where $E = \mid A \mid^2$ is the intracavity normalized dimensionless energy. Again, by using the same method discussed earlier, we can obtain the linear matrix equations. Letting $a(t) = A + \delta a$ and $n(t) = N_0 + \delta n$, the perturbation array $\varepsilon \equiv (\delta a, \delta a^*, \delta n)^T$ is found to obey the linearized equation:

$$d\varepsilon / dt = M\varepsilon, \tag{8}$$

where the eigenmatrix M is

$$M = \begin{pmatrix} M_{11} & M_{12} & M_{13} \\ M_{21} & M_{22} & M_{23} \\ M_{31} & M_{32} & M_{33} \end{pmatrix},$$

with

$$M_{11} = i\delta - in_{Kerr\_N} 2 \mid A \mid^2 + i(N + \sigma_{FCD} N_0^{0.8}) - (1 + \gamma_{FCA} N_0) - 2\alpha_{TPA} \mid A \mid^2,$$

$$M_{12} = -in_{Kerr\_N} A^2 - \alpha_{TPA} A^2,\ M_{13} = i(1 + 0.8\sigma_{FCD} N_0^{-0.2})A - \gamma_{FCA} A,$$

$$M_{21} = M_{12}^*, M_{22} = M_{11}^*, M_{23} = M_{13}^*,\ M_{31} = 2 \mid A \mid^2 A^*,\ M_{32} = M_{31}^*,\ M_{33} = -1/\tau.$$

The complex eigenmatrix M must have two conjugate complex eigenvalues $\lambda_r \pm i\lambda_i$ and one real eigenvalue λ_0. It is well known that for BS condition it requires $\lambda_0 > 0$, while for SP condition $\lambda_r > 0$.

By solving Eqs. (4)- (8), we can analyze various conditions that SP would occur and how strong it is. Besides, physical mechanisms under SP will be discussed below.

For the silicon MRR shown in Fig. 1, we choose a ridge waveguide with a width of 550 nm, a height of 400 nm and a height of ridge of 180 nm. The waveguide has an effective index of 2.99, and effective area of 0.254 μm^2. The use of ridge waveguide has an advantage in reducing the carrier lifetime in the silicon waveguide if a pair of reverse biased p-i-n electrodes is added on both sides of the ridge. The linear loss of the ridge waveguide is about 1 cm^{-1} and the radius is 5μm, resulting in a quality factor of about 60000. When considering critical coupling, the power coupling parameter is about 0.003, and the gap between the ring and bus waveguides is about 780 nm.

Actually, the nonlinear area is slightly smaller than the effective area of the silicon ridge waveguide, therefore we assume the effective area to be approximately the nonlinear area. The

#160644 - $15.00 USD Received 3 Jan 2012; revised 16 Feb 2012; accepted 14 Mar 2012; published 19 Mar 2012

nonlinear volume is assumed to be the product of this nonlinear area and the length of the silicon MRR. Other material parameters are defined as follows: for Kerr coefficient $n_{2I} = 4.5 \times 10^{-18}\text{m}^2/\text{W}$, for TPA coefficient $\beta_2 = 0.75 \times 10^{-11}\text{m/W}$, for FCA coefficient $\sigma_{FCA} = 1.45\times10^{-23} m^2$. $\Delta n_{fc} = -(8.8\times10^{-22}\times N + 8.5\times10^{-18}\times N^{0.8})$ is the refractive index change induced by the FCD effect where N is in cm^{-3} around 1.55μm [25, 27, 28].

3. Analysis and discussion

Although the Kerr effect plays a less important role than the TPA effect on the refractive index change in the wavelength near 1.55 μm, the analysis neglecting Kerr effect in silicon may suffer from the inaccurate prediction of analyzing dynamic unstable processes such as SP and even chaos in silicon waveguides.

In Fig. 2(a), the Kerr effect has negligible influences on the energy in the MRR, particularly for weak input light power. However, it contributes to non-negligible changes in the SP region as indicated by the blue arrows and red circles in Fig. 2(a). Figure 2(b) plots the real eigenvalue λ_0, and the real part of the complex eigenvalues λ_r of the matrix with (blue curves) and without (red curves) the Kerr effect. The threshold energy value for BS and SP is where $\lambda_0 = 0$ and $\lambda_r = 0$, respectively. When the energy in the MRR is very small, the eigenvalue curves of the two matrixes are almost identical, which is known as the linear condition. As the energy in the MRR increases, the eigenvalue curves deviate from each other in most situations, and the energies for the same eigenvalue in these two cases are different. If the Kerr effect is considered, the range of SP extended from (0.77, 1.07) to (0.77, 1.33) in terms of the energy in the MRR or from (3, 34) to (2, 106) in terms of the input light power.

It is clear from the comparison that, although the Kerr coefficient is smaller than the FCD coefficient, the omission of the Kerr effect can be acceptable only in the nonlinear condition where no rapid dynamic process is present (i.e., BS region). The omission of the Kerr effect is inappropriate in analyzing SP or even chaos phenomena. A small perturbation on the refractive index induced by the Kerr effect may have a large impact on SP or chaos, partly due to the fact that the relaxation time for the Kerr nonlinearity is much shorter than the carrier lifetime.

In order to illustrate the parameter ranges of BS and SP clearly, we denote X_{BS}^{+}, X_{BS}^{-}, X_{SP}^{+}, X_{SP}^{-} (X can be E, P, or I_{in}) as the threshold values of the normalized dimensionless energy E, the input power P and the input light intensity I_{in} of the BS and SP, respectively. The superscript sign "+" signifies the onset value, while the superscript sign "-" signifies the cut-off value. It is shown in Fig. 2(a) that $E_{SP}^{-} > E_{SP}^{+} > E_{BS}^{-} > E_{BS}^{+}$, for BS, $P_{BS}^{-} < P_{BS}^{+}$ or $I_{inBS}^{-} < I_{inBS}^{+}$, while for SP, $P_{SP}^{+} < P_{SP}^{-}$ or $I_{inSP}^{+} < I_{inSP}^{-}$. We take the blue lines as an example, under certain conditions, $P_{BS}^{+} > P_{SP}^{+}$ or $I_{inBS}^{+} > I_{inSP}^{+}$. Under such circumstances, if the input light intensity I_{in} satisfies $I_{inBS}^{+} > I_{in} > I_{inSP}^{+}$, the output light intensity is determined by the initial state of the energy in the MRR. If the initial normalized dimensionless energy in the MRR is zero at $t = 0$, the energy keeps staying at the lower branch of the BS curve in Fig. 2(a), and the system will select to give a steady state (CW) output intensity. In contrast, if the initial energy in the MRR is taken as 1 at $t = 0$, the energy will keep staying at the upper branch of the BS curve, and the system will select to output oscillating intensity (i.e., SP). Thus, it can be seen that one input light intensity corresponds to two different output states: one is stable state and the other the oscillating state. This is different from the BS situation where one input light intensity corresponds to two stable output states.

#160644 - $15.00 USD Received 3 Jan 2012; revised 16 Feb 2012; accepted 14 Mar 2012; published 19 Mar 2012

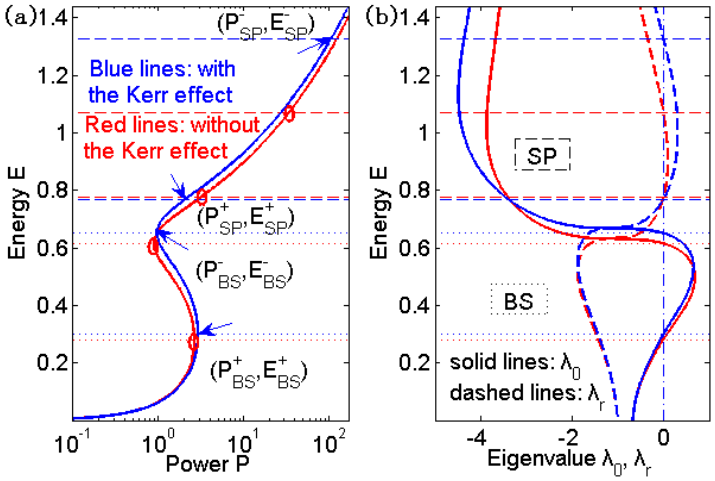

Fig. 2. Left (a): Steady state response E versus input normalized power P with (plotted in blue) and without (plotted in red) the Kerr effect, respectively. Right (b): Real eigenvalue (solid curves) and the real part of the two conjugate complex eigenvalues (bold dashed curves) that with (plotted in blue) and without (plotted in red) the Kerr effect, respectively. The dotted lines indicate BS threshold values; while the fine dashed lines indicate the start and end threshold values of the SP (both of them are plotted in two colors for the cases of with/without the Kerr effect.) Note that the above analyses are carried out for the carrier lifetime of 150ps and the input light wavelength detuning of –0.05nm (if not other specified, the carrier lifetime and the input light wavelength detuning take these values in the following simulations).

Equation (2) can be used to explain why SP occurs. When the input light is strong enough, all of the nonlinear effects-the TPA, FCA, FCD, and Kerr effects-will be involved. SP stems from the interaction between the resonance frequency of the MRR and the light intensity in the MRR. For example, we take the resonance wavelength of the MRR as the wavelength of the input light. In this case, the light intensity in the MRR increases gradually, and the absolute value of the refractive index change induced by the Kerr and FCD effects increases too, but with the opposite directions. As is pointed out that the FCD effect takes the major role in controlling refractive index over the Kerr effect, the total refractive index would become smaller, which blue-shifts the resonance wavelength. As a result, the input light wavelength is not the exact resonance wavelength any more at this moment and the total light in the ring will gradually decrease. The decrease of light intensity in the MRR would reduce the TPA induced non-equilibrium carrier concentration, which contributes to the increase of the refractive index as well as the red-shift of the resonance wavelength to align more closely with the input light wavelength. This process increases the intracavity light intensity again. If the two competitive processes progress with time, SP will occur. However, as indicated by our simulations, the carrier lifetime must be as the same order of magnitude as the photon lifetime in the MRR for the occurring of SP.

#160644 - $15.00 USD Received 3 Jan 2012; revised 16 Feb 2012; accepted 14 Mar 2012; published 19 Mar 2012

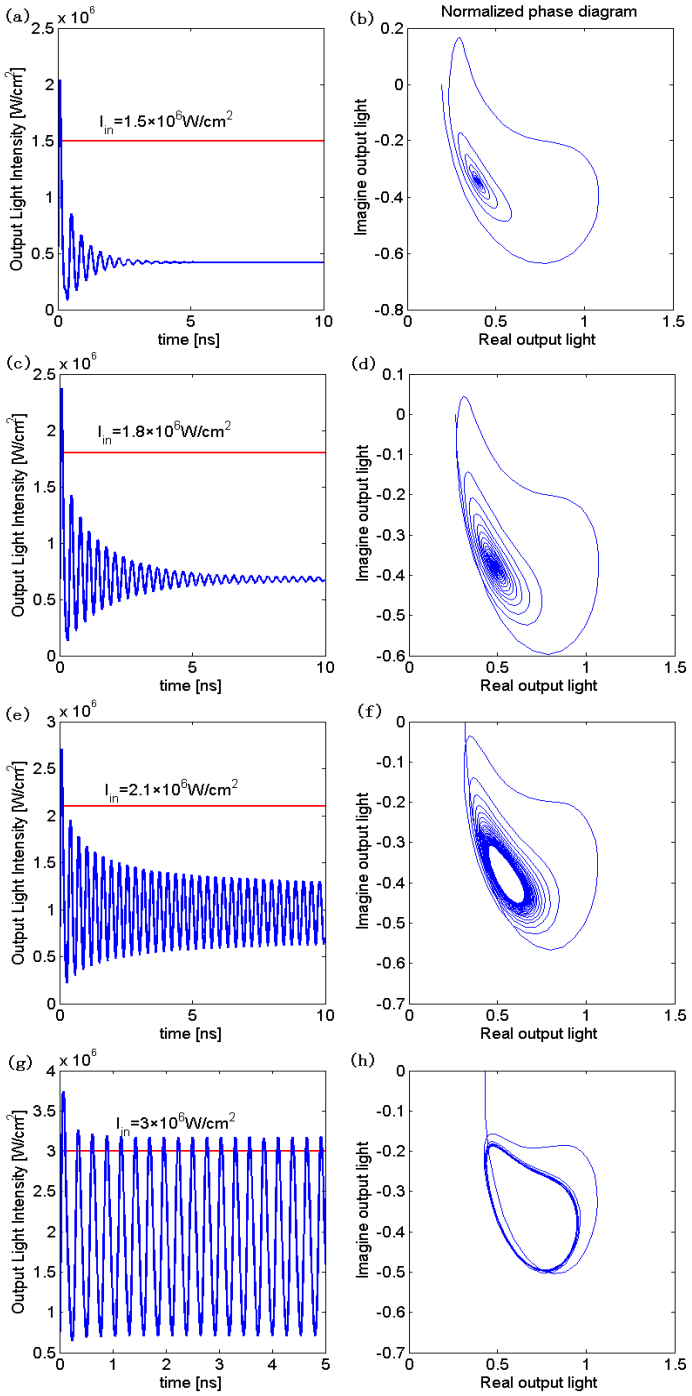

Fig. 3. Output light intensities in time domain with different input intensities (a), (c), (e), (g) and their associated phase loops (b), (d), (f), (h). The phase loop of the output light is normalized according to the input light.

As is illustrated in Fig. 3, when the input light intensity is less than $1.5 \times 10^6 W/cm^2$, no oscillation appears for the output light intensity. With increasing the input light intensity, the oscillation becomes stronger as is clearly seen from Fig. 3(c) to 3(f). When the input light

#160644 - $15.00 USD Received 3 Jan 2012; revised 16 Feb 2012; accepted 14 Mar 2012; published 19 Mar 2012

intensity is much higher (see Fig. 3(g) and 3(h)), the time required for the build-up of SP becomes short, so does the oscillation period. The phase-space pictures of the output light are also shown in Fig. 3, which shows the attracting limit cycle (here we call it as phase loop). A stable phase loop suggests a periodic oscillation which is called SP. If the SP oscillation waveform is a simple harmonic wave, i.e., sinusoidal or cosine functions, the phase loop should be a perfect round loop. The roundness of the loop reflects the simple harmonic oscillation degree of the SP oscillation. That is, the second and higher harmonic oscillations will appear when the phase loop is not a perfect round circle: the more serious the loop deviates from the round circle, the larger the second and higher harmonic oscillation components are in the SP oscillation. Furthermore, the larger the loop is, the larger the amplitude of the SP will be.

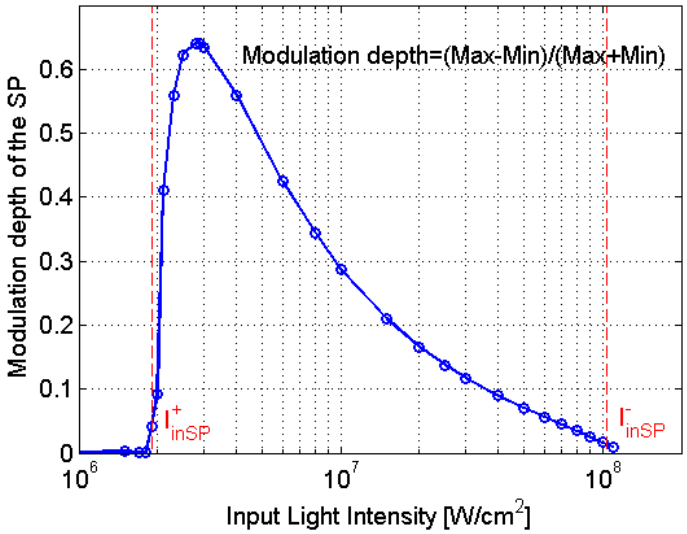

Fig. 4. Modulation depth of SP versus input light intensity. The modulation depth of SP is defined as the difference between the maximum and minimum output light intensity divided by their sum. The two red dashed lines indicate SP threshold values, denoted as I^{+}_{inSP} and I^{-}_{inSP}.

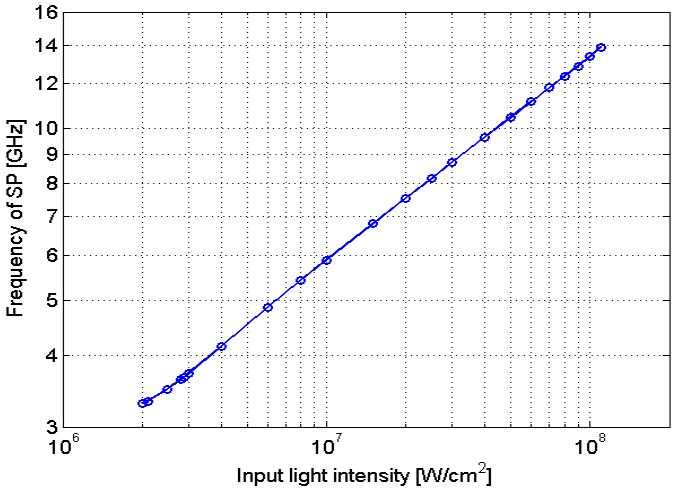

Fig. 5. SP frequency versus input light intensity (in logarithmic coordinates).

#160644 - $15.00 USD Received 3 Jan 2012; revised 16 Feb 2012; accepted 14 Mar 2012; published 19 Mar 2012

The modulation depth of the SP is restricted by the MRR's inner energy, the carrier density and the carrier lifetime. With the increasing of the input light intensity the modulation depth of the SP increases rapidly at first, after reaching a peak point, it decreases gradually, as illustrated in Fig. 4. Here we take the input light intensity of 3×10^6W/cm^2 and 3×10^7W/cm^2 respectively for instance. According to the calculation, when the carrier lifetime is 150ps and the linear loss is 1 cm^{-1}, the normalized dimensionless carrier lifetime is determined to be about 1.5. As the input light intensity is 3×10^6W/cm^2, the output light intensity oscillates between 0.714×10^6W/cm^2 and 3.172×10^6W/cm^2 with the modulation depth 0.633. In contrast, as the input light intensity is 3×10^7W/cm^2, the output light intensity oscillates between 2.5×10^7W/cm^2 and 3.15×10^7W/cm^2, showing a modulation depth of only 0.115.

As shown in Fig. 5, the SP frequency increases with the enhancing of the input light intensity. The fitting function between the SP frequency and the input light intensity is $\log(f) = a + b*\log(I_{in})$, where $a = -1.7745$ and $b = 0.3628$, where the unit of f is GHz and I_{in} is W/cm^2. We can find that in logarithmic coordinates, the relation between the SP frequency and the input light intensity is linear. Besides, it is also found that when the input light intensity, the carrier lifetime and the linear loss are fixed, the SP frequency takes the same value for any input light wavelength.

It has been proved that the SP can occur only when the varying range of $|a|^4$ and n/τ are in the same order of magnitude and have overlapping values, which requires that the carrier lifetime must be within a specific range. As can be seen in Fig. 6 that the input light intensity I_{inSP}^{+} for the onset point of the SP declines when the carrier lifetime increases up to approximately 150ps and then increases slowly with the further increasing of the carrier lifetime. On the other hand, the input light intensity I_{inSP}^{-} for the cut-off point of the SP always goes down with the increasing of carrier lifetime. Obviously there exists a critical carrier lifetime (about 260 ps) beyond which the output light cannot oscillates by all means. As shown in Fig. 4, since the modulation depth of the SP near I_{inSP}^{-} is fairly small, it is hard to observe prominent SP phenomenon near the critical carrier lifetime value.

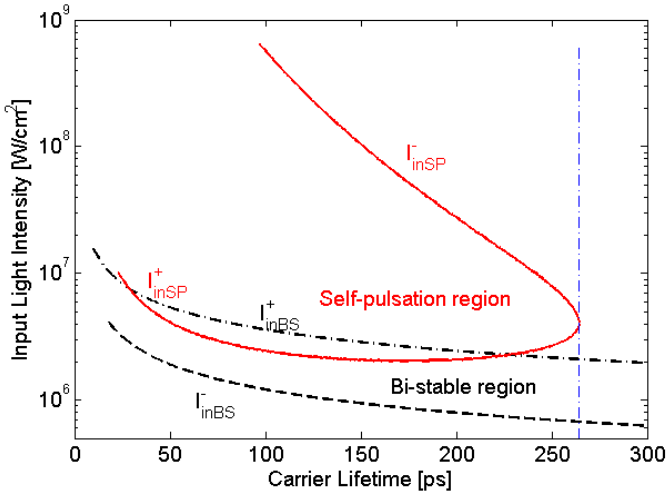

Fig. 6. Threshold value of the input light intensity for BS and SP versus carrier lifetime. SP has a cut-off carrier lifetime of about 260ps, while BS has a more wider carrier lifetime range.

From Fig. 6 we can find the influence of carrier lifetime on BS as well. The input light intensity required for BS always declines as increasing the carrier lifetime. In general, the carrier lifetime in the silicon MRR is several ns or even larger. This may be the main reason many research groups up to now have successfully observed BS but seldom observe SP

#160644 - $15.00 USD Received 3 Jan 2012; revised 16 Feb 2012; accepted 14 Mar 2012; published 19 Mar 2012

phenomenon, which needs much shorter carrier lifetime and much higher input light intensity. However, some research groups have demonstrated experimentally that the carrier lifetime can be reduced to tens or hundreds of picoseconds by adding a reverse biased p-i-n electrodes on both sides of the MRR waveguide structure to deplete free carriers, or implanting ions in the center of waveguide as the killer of free carriers [29–31]. This method could be employed to demonstrate SP in silicon MRR.

As illustrated in Fig. 7, in general, the BS and SP mainly occur in the wavelength region where the input light wavelength having a negative detuning with respect to the critical coupling wavelength of the MRR. This is because the TPA and FCD effects always blue-shift the critical coupling wavelength of the MRR. However, there exists an interesting exception, which is not intuitional and difficult to explain at present, that SP can also occur when the input light wavelength has a positive detuning, as well as much higher input light intensity and relative shorter carrier lifetime. In fact, the wavelength limit (or cut-off wavelength) and input light intensity regions for SP have a nonnegligible dependence on the carrier lifetime, namely, the region will become narrower with the increase of the carrier lifetime. On the contrary, for BS, the carrier lifetime contributes less to the cut-off wavelength and the input light intensity range.

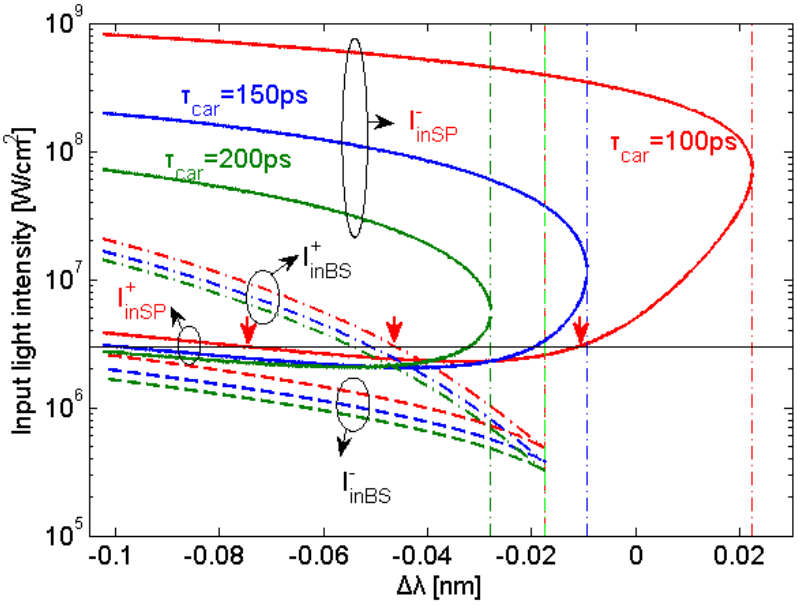

Fig. 7. Threshold input light intensity regions of BS and SP versus input wavelength detuning and different carrier lifetimes 100ps (red lines), 150ps (blue lines) and 200ps (green lines), respectively. Solid curves are SP threshold lines, whereas dashed and dashed-dot curves refer to BS threshold lines.

At steady state, the output optical spectra with different input light intensities (all below the input light intensity threshold for the onset of SP I_{inSP}^{+}) are shown in Fig. 8. As the input light intensity is lower than 5×10^4W/cm^2, the optical spectrum shows a minimum output light intensity at the linear resonant wavelength of the MRR. With the increasing of the input light intensity, the resonant wavelength is blue-shifted, and the extinction ratio decreases as well. Furthermore, the spectrum is not symmetric any more. As the input light intensity is larger than 5×10^5W/cm^2, BS will occur, as shown by the dash-dot lines in the figure. Due to BS, the output light intensity has two stable values, depending on the initial MRR intra-cavity energy. The output versus input light intensity curve is also plotted in the inset of Fig. 8, which agrees

#160644 - $15.00 USD Received 3 Jan 2012; revised 16 Feb 2012; accepted 14 Mar 2012; published 19 Mar 2012

quite well with the black curves when the input light intensity is 1×10^6W/cm^2 and the wavelength detuning is –0.03nm.

As shown in Fig. 7, when the input light intensity is in the region between I_{inSP}^{+} and I_{inBS}^{+}, the state of the output light (stable or oscillating) is determined by the initial energy state in the MRR. In order to describe the SP phenomenon in wavelength domain, the instantaneous optical spectrum is plotted as shown in Fig. 9, where different colors represent different time points of one SP oscillating circle. When the initial light energy in the ring is too small, an input light intensity I_{in} as large as 3×10^6W/cm^2 ($I_{inSP}^{+} < I_{in} < I_{inBS}^{+}$) cannot switch the MRR intra-cavity energy E onto the upper energy branch. As a result, the energy E is stable and the output light is still a stable CW. This is shown in Fig. 9(a) where the blue-shift of the input wavelength is larger than 0.0463nm ($\Delta\lambda$<-0.0463nm). The cut-off wavelength detuning points of the SP in Fig. 9(a) agree well with the intersection points of the black line and the red lines in Fig. 7, i.e. the point (–0.01nm, 3×10^6W/cm^2) and point (–0.0463nm, 3×10^6W/cm^2) which are indicated by red arrows. Note that only the first and second intersection points from right to left are the correct ones due to the initial state (a, n) = (0, 0). If the initial energy in the MRR is not zero, just as the case that a high-power narrow laser pulse is used to stimulate the MRR energy to be larger than E_{SP}^{+} (i.e., the initial state (a, n) = (1, 1.5)), the same input light intensity I_{in} will switch the MRR energy onto the SP state, and the output light intensity will oscillate as well. As shown in Fig. 9(b), the output light keeps oscillating in the wavelength detuning range of (–0.076nm, –0.01nm). The cut-off wavelength detuning points of the SP in Fig. 9(b) agree well with the first and third intersection points of the black line and the red lines in Fig. 7, i.e. the point (–0.01nm, 3×10^6W/cm^2) and point (–0.076nm, 3×10^6W/cm^2) which are indicated by red arrows.

It is worth noting that in Fig. 9(a), when the input light wavelength is close to the cut-off blue-shifted wavelength detuning value –0.0463nm, an extremely small change of the input wavelength will generate a large change of the output intensity. Since in reality a laser with infinite narrow linewidth does not exist, any small random perturbation on the laser's wavelength will arise irregular oscillations which shows a non-periodic nature in the time domain – a typical behavior of the chaotic state. Therefore, we predict that the output light state of the nonlinear MRR undergoes a chaos state when the nonlinear MRR transits from BS to SP.

Figure 10 illustrates the relationship between input light intensity for SP and BS and waveguide linear loss. The input light wavelength is detuned from the central resonant wavelength peak of the MRR to the short wavelength end by 3dB. When the linear loss is larger than 1.8cm^{-1}, SP will disappear but not for BS, regardless how high the input light intensity is. However, with the increase of the linear loss, the Q factor will decrease and the 3dB bandwidth will increase as well. As a result, the required input light intensity for BS must be increased to ensure the enough refractive index change.

Finally, through simulation we also find that when enlarging the radius of the ring, SP onset input light intensity I_{inSP}^{+} increases linearly with respect to radius. When fixing the linear loss coefficient, the total loss of a larger ring is higher than that of a smaller one. Therefore the critical coupling coefficient between the ring and the input/output waveguide for the larger ring should be enlarged. It is known that the total energy enhancing factor of a MRR is reversely proportional to its power coupling coefficient. Only by increasing the input light intensity, can the energy in a larger ring be guaranteed to be equal to that in a smaller one. This is the reason why a larger MRR needs more input light intensity to stimulate the SP.

#160644 - $15.00 USD Received 3 Jan 2012; revised 16 Feb 2012; accepted 14 Mar 2012; published 19 Mar 2012

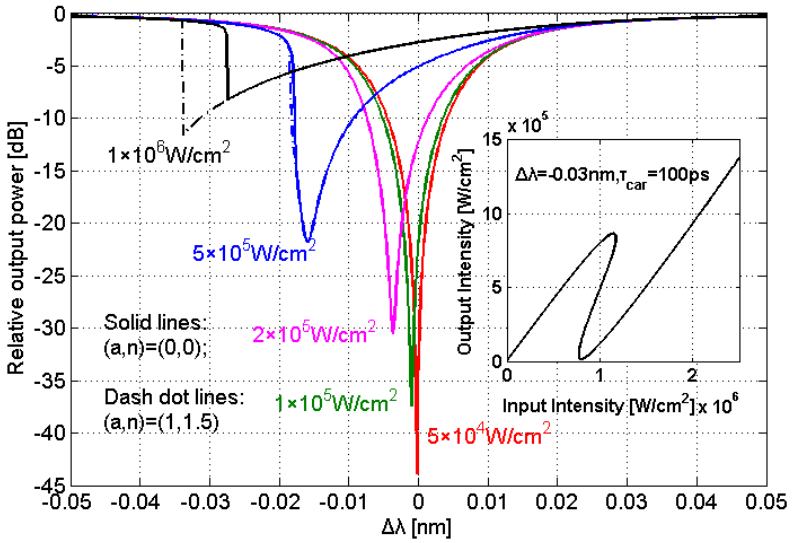

Fig. 8. Optical spectra of the output light for different input light intensities. This picture illustrates the relationship between the relative output intensity (the output light intensity divided by the input light intensity in dB) and the input wavelength detuning in different input light intensities. Inset: Output light intensity versus input light intensity when omitting SP. When the input light is 1×10^6W/cm^2 and the wavelength detuning is –0.03nm, there are two output states shown in this figure, which fits well with the black curves. Note that the carrier lifetime in this case is 100 ps.

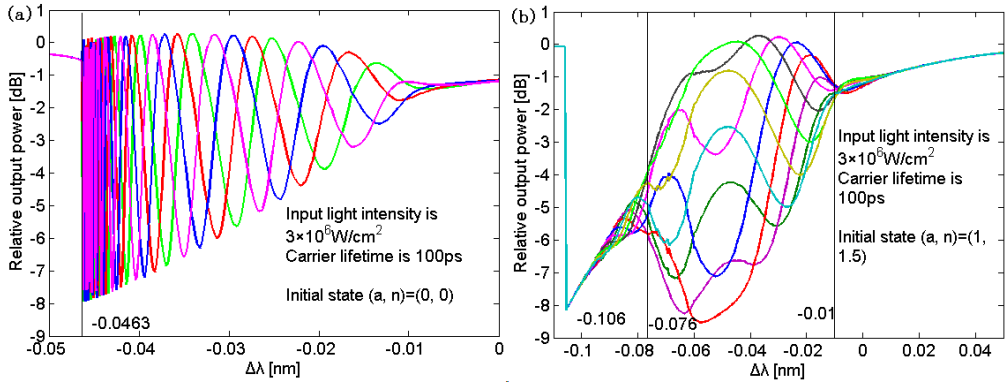

Fig. 9. Optical spectra at different time points (plotted in different colors). These time points are sampled evenly within one SP oscillating circle. (a): the normalized dimensionless energy and carrier density in the MRR at initial state are both 0. (b): the normalized dimensionless energy and carrier density in the MRR at initial state are 1 and 1.5, respectively. This figure is obtained by calculating the output intensity at the fixed time of each wavelength detuning. In (a), there are four fixed time points from 22.4 ns to 22.55 ns. In (b), there are nine points from 22.4 ns to 22.625 ns with 0.025 ns time interval. The waveguide dispersion and material dispersion are omitted due to the narrow wavelength detuning.

#160644 - $15.00 USD Received 3 Jan 2012; revised 16 Feb 2012; accepted 14 Mar 2012; published 19 Mar 2012

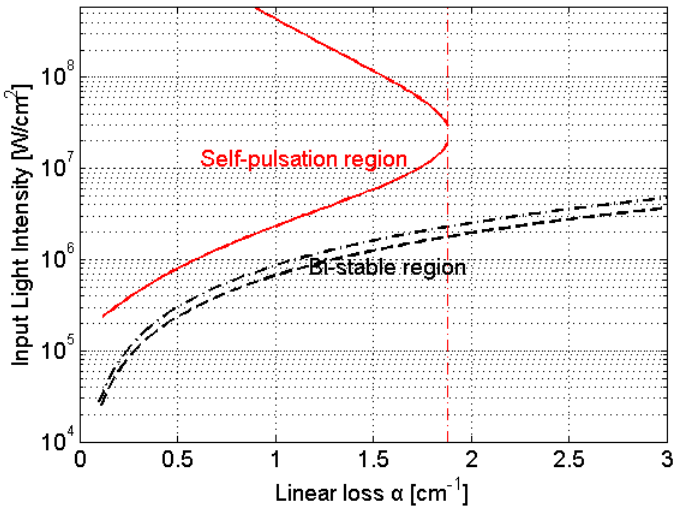

Fig. 10. Input light intensity regions for BS (I_{inBS}^{+} , I_{inBS}^{-}) and SP (I_{inSP}^{+} , I_{inSP}^{-}) versus the linear loss of the MRR. The input light wavelength detuning is chosen to be $-\Delta_{3dB}$. The carrier lifetime is fixed at 100ps.

4. Conclusions

We have established the normalized dimensionless nonlinear equation and the carrier density equation based on both the Kerr and the TPA nonlinear optical effects (the FCA and FCD effects induced by the TPA are also included) which describe the complicated dynamics of a silicon MRR and studied the BS and SP phenomena in the MRR. By using stable analysis method for differential equations, input light intensity ranges for the BS and the SP have been given. Some of the important conclusions are summarized as follows.

Although the coefficient of the Kerr effect is much smaller than that of the TPA and FCD, it also plays an important role on SP, especially on controlling the operation range of SP.

SP phenomenon can be observed when the input light intensity is about 3×10^6 W/cm^2 (corresponding to the input power of approximate 7.6 mW) with the carrier lifetime ranging from 70ps to 250ps. It should be pointed out that the initial energy in the MRR affects the final output light intensity: in some region of parameters, one input state may result in two different output states: stable and oscillating. This is quite different from the BS situation where one input state corresponds to two stable output states;

SP frequency shows a linear dependence on the input light intensity in logarithmic coordinates, which can be adjusted from several GHz to higher than tens of GHz;

The modulation depth of SP is changed with the input light intensity. The optimal input light intensity for the largest modulation depth locates near the onset threshold value of the SP;

The cut-off input wavelength detuning value of BS has little relationship with the carrier lifetime, whereas the cut-off value of SP changes largely with the carrier lifetime;

With the initial energy state of the MRR being zero, the SP has an extremely sensitive relationship with the blue-shifted detuning of the input wavelength, especially near the cut-off wavelength detuning, and in time domain the output light would enter a chaotic state;

In order to observe the SP with low input light intensity, the linear loss of the MRR should be as low as possible and the radius of the MRR should be as small as possible.

For the silicon MRR, the required input light intensity for SP is in the range of 10^6-10^8W/cm^2, which is well below the optical damage threshold value of 1-4GW/cm^2 for silicon materials [32]. However, in order to avoid heat accumulation in the MRR, the input light duration should not be too long, for example less than 0.1 μs. Of course, the method

#160644 - $15.00 USD Received 3 Jan 2012; revised 16 Feb 2012; accepted 14 Mar 2012; published 19 Mar 2012

employed in this paper for analyzing the BS and the SP of nonlinear silicon MRRs can also be applied to other materials based MRRs, such as GaAs and InP.

Acknowledgments

This work is supported by the State Key Development Program for Basic Research of China (Grant No. 2007CB613405), and the National Natural Science Foundation of China (Grant No. 60877013, 61021003 and 60837001).

#160644 - $15.00 USD Received 3 Jan 2012; revised 16 Feb 2012; accepted 14 Mar 2012; published 19 Mar 2012